Hydrolysis embrittles poly(lactic acid)

Meixuanzi Shi,† Quan Jiao,† Tenghao Yin, Joost J. Vlassak,* and Zhigang Suo*

The backbones of biodegradable and bioderived polymers often contain chemical bonds, such as ester and amide that are susceptible to hydrolysis. Here, we show that hydrolysis causes a transition from ductile to brittle fracture in poly(lactic acid) (PLA). Submerged in an aqueous solution and bearing a load, a sample with a precrack undergoes extensive plastic deformation when the crack grows fast, but negligible plastic deformation when the crack grows slowly. In the former, the ductile fracture creates rough and porous crack surfaces, indicating that polymer chains slip before scission. In the latter, the brittle fracture creates flat crack surfaces, indicating that polymer chains slip negligibly before scission. Furthermore, at a low load and over a broad range of pH, the velocity of a crack in PLA correlates with the rate of hydrolysis of lactic acid oligomers. Taken together, these observations demonstrate that PLA suffers hydrolytic embrittlement. The phenomenon should be taken into account in the design of—and with—biodegradable and bioderived polymers.

Impact statement

In thermoplastics of high molecular weights, repeat units form long polymer chains by chemical bonds, and the long polymer chains form solids by physical interactions. Between neighboring repeat units, the chemical bonds are commonly much stronger than the physical interactions. Polymer chains slip extensively before scission in ductile fracture, but slip negligibly before scission in brittle fracture. In biodegradable and bioderived thermoplastics, repeat units often link by chemical bonds susceptible to hydrolysis. Here, we show that hydrolysis embrittles a leading bioderived thermoplastic, poly(lactic acid). Even a small load exposes a crack tip to water molecules from the environment, hydrolyzing ester bonds and breaking chains with negligible chain slip. The material has a toughness above 10^4 J/m^2. However, submerged in an aqueous solution, the material can grow a crack at an energy release rate as low as 1 J/m^2. Hydrolytic embrittlement should be investigated for biodegradable and bioderived polymers under development for health care and sustainability.

Introduction

Poly(lactic acid) (PLA), commonly derived from corn and sugarcane, is a leading biodegradable polymer.[1,2] PLA is a polyester that undergoes hydrolysis in moist environments.[1,3] The hydrolysis is slow enough to allow PLA to be used in applications traditionally reserved for plastics derived from petroleum, but fast enough to serve as a mechanism of biodegradation for some single-use products. The range of applications of PLA has been growing; examples include deli trays,[4] packaging,[5,6] medical implants,[7,8] and 3D printing.[9,10] It was discovered recently, however, that PLA can grow cracks at appreciable velocities even at low loads.[11] A small load opens a crack and allows water molecules to react with the ester bonds at the crack tip. Such hydrolytic cracks can greatly outrun degradation, and raise reliability concerns. Hydrolytic cracking has been reported in medical sutures made of another biodegradable polyester, poly(glycolic acid).[12] The behavior of hydrolytic cracking should be fully characterized to enable wider applications of PLA. Moreover, intense efforts are ongoing to develop biodegradable and bioderived polymers, the backbones of which are commonly susceptible to hydrolysis.[13–15] PLA may serve as a model material to study hydrolytic cracking of such polymers.

Historically, similar environmentally assisted cracking has been studied in many other materials, including metals,[16,17] oxides,[18–20] and polymers with unsaturated carbon bonds (e.g., natural rubber[21,22]). This long-standing fielding was recently rejuvenated by its relevance to biodegradable and

Meixuanzi Shi, John A. Paulson School of Engineering and Applied Sciences, Harvard University, Cambridge, USA; State Key Laboratory for Strength and Vibration of Mechanical Structures, Department of Engineering Mechanics, Xi'an Jiaotong University, Xi'an, China
Quan Jiao, John A. Paulson School of Engineering and Applied Sciences, Harvard University, Cambridge, USA; qjiao@seas.harvard.edu
Tenghao Yin, John A. Paulson School of Engineering and Applied Sciences, Harvard University, Cambridge, USA; State Key Laboratory of Fluid Power & Mechatronic Systems, Key Laboratory of Soft Machines and Smart Devices of Zhejiang Province, Center for X-Mechanics, and Department of Engineering Mechanics, Zhejiang University, Hangzhou, China
Joost J. Vlassak, John A. Paulson School of Engineering and Applied Sciences, Harvard University, Cambridge, USA; vlassak@seas.harvard.edu
Zhigang Suo, John A. Paulson School of Engineering and Applied Sciences, Harvard University, Cambridge, USA; suo@seas.harvard.edu
*Corresponding author
†These authors equally contributed to this work.
doi:10.1557/s43577-022-00368-5

© The Author(s), under exclusive license to the Materials Research Society 2022

biomedical materials. Several studies have reported hydrolytic growth in degradable elastomers, for example, poly(glycerol sebacate)[23] and poly(dimethylsiloxane).[24,25] A recent review by Baumberger et al.[26] discussed various aspects of environmental control of crack propagation in hydrogels.

A thermoplastic polymer fractures by two molecular processes: slip between polymer chains and scission of polymer chains.[27–31] Depending on temperature, strain rate, and chemical environment, the polymer can fracture by chain scission without chain slip (**Figure 1**a), by chain slip without chain scission (Figure 1b), or by chain slip and chain scission (Figure 1c).

For the PLA used in this work, when a sample without precrack is stretched, polymer chains slip before scission (Figure 1c). The repeat units of PLA and water molecules have high energy of mixing, so that the concentration of water molecules in PLA is low, and hydrolysis is negligible during the experiment.[32,33] Similarly, when a sample with a precrack is stretched with a large load, hydrolysis is still negligible, and the crack advances rapidly, surrounded by a large zone of plastic deformation. In both cases, the fracture surfaces are rough and porous.

Here, we show that hydrolysis can cause the PLA to fracture by chain scission without chain slip (Figure 1a). A previous study showed that PLA is susceptible to hydrolytic cracking and that the crack velocity is sensitive to humidity and pH.[11] The previous work did not examine the fracture surfaces, and the range of energy release rate tested was narrow, 1100–1450 J/m^2, within which the crack velocity was nearly constant. To demonstrate fracture by chain scission without chain slip, here we test samples using a wide range of energy release rates, 1–10,000 J/m^2, in aqueous solutions of a wide range of pH, 1–12. We also examine fracture surfaces using a scanning electron microscope (SEM). Depending on energy release rate and pH, the crack velocity varies by orders of magnitude. At high energy release rates, a crack grows fast and plastic deformation is extensive, producing porous and rough fracture surfaces, indicating fracture by a combination of chain slip and chain scission. At low energy release rates, a crack grows slowly and plastic deformation is negligible, producing flat fracture surfaces, indicating fracture by chain scission with negligible chain slip. Given an energy release rate, a crack grows faster in acidic and basic solutions than in a neutral solution. This behavior correlates with the rate of hydrolysis of lactic acid oligomers. Taken together, these observations demonstrate that hydrolysis of PLA turns a ductile polymer into a brittle one.

Materials and methods

This study was performed using a commercial poly(L-lactic acid) film (Goodfellow #247-628-87) with a thickness of 50 μm. According to the description provided by the manufacturer, the film is processed by biaxial stretching. Because the film is a commercial material, more detailed information on composition and processing is unavailable. We characterize the film using differential scanning calorimetry (TA Instrument Discover 250). A "heat-cool-heat" program is used to scan the sample over a temperature range of 25–200°C at a rate of 5°C/min.

For the uniaxial tensile test, we prepare dog-bone-shaped specimens, gauge length 12 mm and width 2 mm, according to the ISO 527-2-5B standard, using a sample cutting die (Ace steel rule dies). The film thickness is measured using both a digital thickness gauge (Clockwise Tools DTNR-055) and a micrometer (Mitutoyo MDC-1 SFB). The tensile specimens are deformed using a tensile tester (Instron 5966) with a crosshead velocity of 0.1 mm/s. During the tensile experiments, the force is recorded at a frequency of 20 Hz.

To study crack growth, we prepare single-edge notch tensile (SENT) specimens with a width of 40 mm and a height of 120 mm. A precrack with a length of 10 mm is introduced using a razor blade. Acrylic clamps are glued to the short edges of the SENT specimens. For the critical

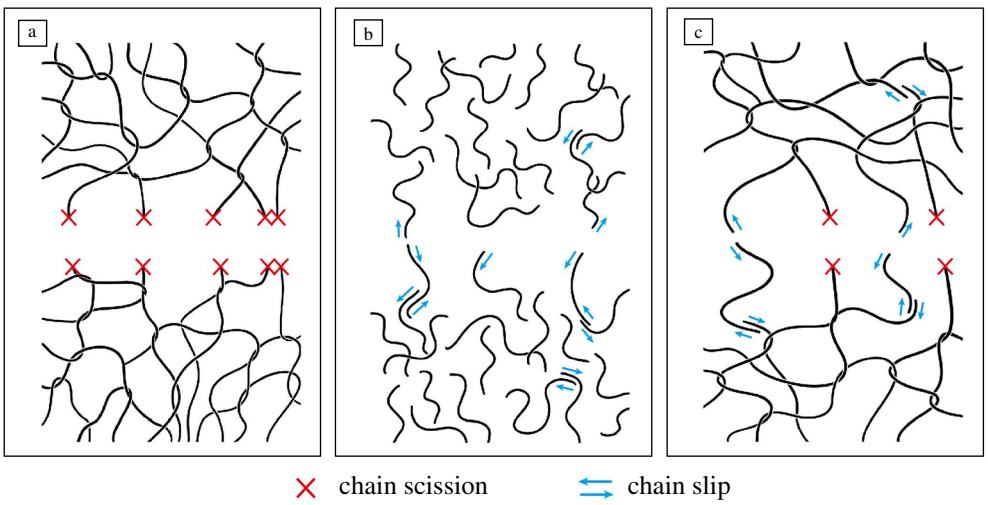

Figure 1. Molecular processes of fracture of thermoplastic polymers. (a) Fracture by chain scission without chain slip. (b) Fracture by chain slip without chain scission. (c) Fracture by chain slip and chain scission.

fracture experiments, the SENT specimens are pulled by a tensile tester (Instron 5966) with a crosshead velocity of 0.1 mm/s, while the force is recorded at a frequency of 20 Hz. In the hydrolytic fracture experiments, a constant force is applied to the SENT specimens using a dead weight of mass m. The net tensile force on the sample is the weight of the mass minus the buoyancy force,

$$F = \frac{\rho_m - \rho_w}{\rho_m} mg, \qquad 1$$

where the density of the hanging mass is $\rho_m = 7.5$ g/cm^3, the density of all aqueous solutions is assumed to be $\rho_w = 1.0$ g/cm^3, and $g = 9.8$ m/s^2 is the gravitational acceleration. The mass is attached to the bottom acrylic clamp using a stainless-steel clip, and a pair of thin silicone rubber pads are glued to both sides of the acrylic clamps to prevent the clip from sliding when the applied mass exceeds 1 kg. Because the total mass of the acrylic and silicone rubber is only ~5 g and their densities ~1.2 g/cm^3 are close to that of the solution, we ignore their contribution to the total tensile force.

During the hydrolytic fracture experiments, we record crack length as a function of time using a digital microscope (Celestron Digital Microscope Pro). The microscope has a working distance of a few centimeters and can image a field of view a few centimeters across with a resolution better than 100 μm. The crack velocity, v is obtained from the derivative of the crack length with respect to time.

We measure the hydrolytic crack growth by submerging specimens in aqueous environments of various pH. We use deionized water as an aqueous environment with a nominal pH 7. The DI water absorbs carbon dioxide from the air, which reduces its pH value. Our measurements indicate that the pH of DI water reduces from 7.5 to 7.1 in one week. For practical purposes, in this work we label the tests done using DI water simply by pH 7. In all other tests, pH values are set by the buffered solutions. The solution of pH 12 is made by dissolving 0.4 g of sodium hydroxide (S8045, Sigma-Aldrich) in 1 L of deionized water. Buffered solutions are used to maintain stable pH 1, 4, 10. The buffered solution of pH 10 is prepared by mixing 183 mL of 0.1 M sodium hydroxide solution and 4.77 g of sodium tetraborate decahydrate (S9640, Sigma-Aldrich) and adding deionized water for a total volume of 1 L. The buffered solution of pH 4 is prepared by mixing 1 mL of 0.1 M hydrochloric acid (HX0603-3, Millipore Sigma), 10.21 g of potassium hydrogen phthalate (P1088, Millipore Sigma), and deionized water for a total volume of 1 L. The buffered solution of pH 1 was obtained by mixing 670 mL of 0.2 M hydrochloric acid, 3.73 g of potassium chloride (6858, Mallinckrodt), and deionized water for a total volume of 1 L. pH values are periodically monitored using a pH meter (Aperta Instruments PH60) to ensure that pH variations stay within ± 0.1 for all experiments in acidic and basic environments.

To prepare for scanning electron microscope imaging (Zeiss Ultra Plus), the fractured specimens are gently rinsed using deionized water and dried in air. To prevent charging during imaging, a 5-nm coating of $Pt_{80}Pd_{20}$ alloy is deposited on the specimens using a sputter coater (EMS 150 T S metal sputter coater). The fracture surfaces are examined at an accelerating voltage of 3 kV.

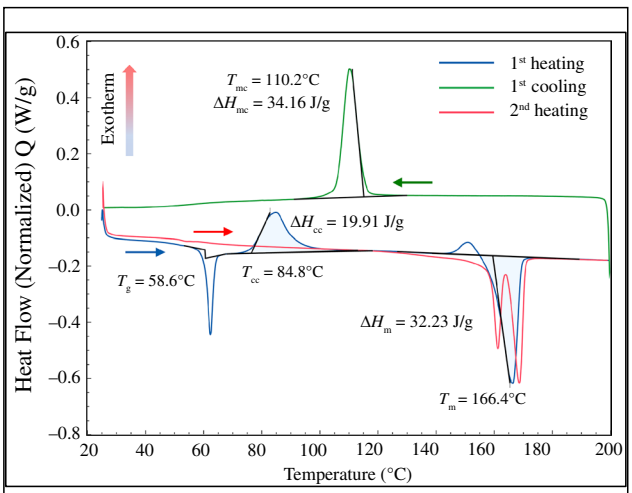

Figure 2. Differential scanning calorimetry scan of the PLA film used in this study. The heating-cooling-heating cycle is performed at a rate of 5°C/min.

Results

Differential scanning calorimetry (DSC)

Figure 2 shows a typical differential scanning calorimetry scan of the PLA film used in this study. The result of the first heating scan shows that the film has a glass-transition temperature $T_g = 58.6$°C, a cold crystallization temperature $T_{cc} = 84.8$°C, and a melting temperature $T_m = 166.4$°C. The degree of crystallinity of the as-received film is determined by

$$X = \frac{\Delta H_m - \Delta H_{cc}}{\Delta H_{f0}}, \qquad 2$$

where ΔH_m and ΔH_{cc} are the enthalpies associated with melting and cold crystallization, and ΔH_{f0} is the specific enthalpy of fusion (93 J/g) for PLA crystals.[34] The degree of crystallinity of the PLA in the as-received state is 13.3 percent. During cooling, the PLA crystallizes at 110.2°C with a large change in enthalpy, indicating that, at the cooling rate used in the DSC scan, the sample crystallizes more completely than the as-received film. Consequently, in the second heating scan, no cold crystallization is observed. The large endothermic peak near 60.5°C in the first heating scan indicates a high level of physical aging of the as-received film during the heating scan, but this peak is absent in the second heating cycle, suggesting that the as-received film was cooled much faster during processing than the scan rate of 5°C/min used for the DSC measurement. The second heating scan shows two melting peaks, which are associated with the melting of disordered and

ordered phases. Such phase separation is commonly observed in PLA with a high L-lactic content.[35]

Tensile test

Consider a sample under uniaxial tension (Supplementary Video 1). Along the stress–strain curve we mark several states of deformation (**Figure 3**a). As the crosshead moves, the stress rises steeply and peaks at a strain of 0.03. Associated with the peak stress, one end of the sample whitens. The nucleation site of the whitening is likely due to stress concentration. Subsequently, the white zone spreads along the sample, while the stress decreases gradually. At a strain of 0.09, a neck becomes evident to the naked eye. At a strain of 0.37, the neck has reached a constant width and propagates along the sample, while the stress plateaus. At the constant stress, the sample does not deform further in either the necked or unnecked region, and the motion of the crosshead is entirely accommodated by propagation of the neck. At a strain of 2.90, the neck reaches the other end of the sample, leaving the sample with a uniform width. Subsequently, the stress rises again, and the sample deforms uniformly, before it ruptures at a strain of 3.30.

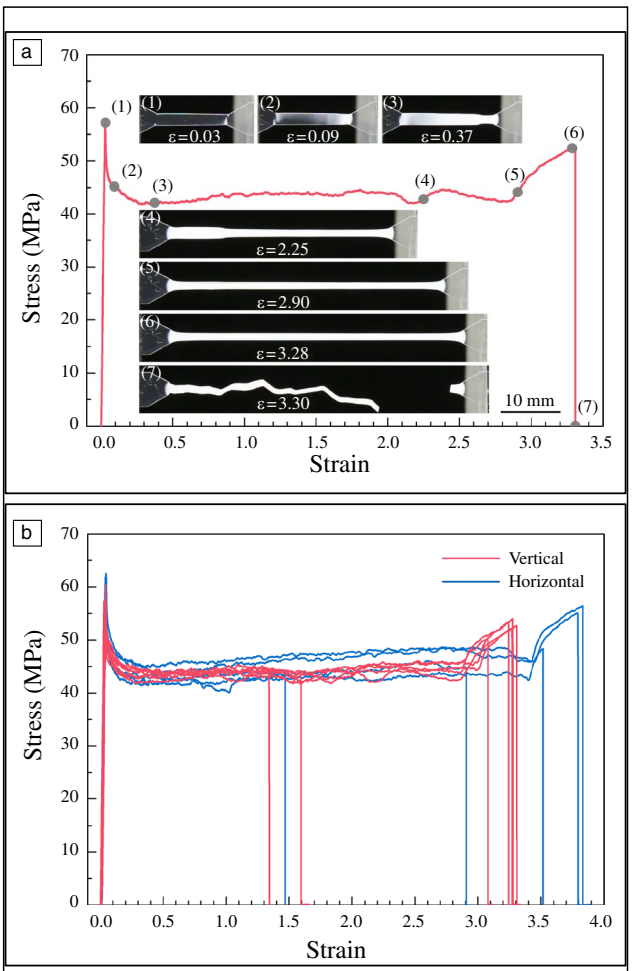

Figure 3. Uniaxial tensile test. (a) Stress–strain curve of a sample, along with snapshots at several strains. The stress is defined by the force divided by the area of the sample in the undeformed state, and the strain is defined by the displacement of the crosshead divided by the gauge length of the sample in the undeformed state. (b) Stress–strain curves of multiple samples. The red and blue curves correspond to samples cut from the as-received film in two perpendicular directions parallel to the edges of the film.

It is known that whitening results from cavitation.[36] We measure the dimensions of the deformed sample. The unnecked white region changes thickness, width, and length slightly, and thus changes volume slightly. In the necked region, however, the width changes from 2 to 1.45 mm, and the thickness changes from 0.050 to 0.028 mm. The sample fractures at a tensile strain of 3.30. Consequently, the volume of the necked region is 1.74 times the undeformed material. This observation is consistent with cavitation before fracture.

We have repeated the uniaxial tensile test using a large number of samples (Figure 3b). The as-received film has a square shape. We cut dogbone samples with gauge length parallel to the two edges of the film, and label them as horizontal and vertical directions. Some samples rupture before the neck reaches the other end of the sample. In such cases, the sample typically ruptures near the front of the neck, possibly when the front of the neck meets a defect in the sample. For the six samples cut from the film in the vertical direction, two samples rupture before the necks propagate through the entire samples, and the other four samples rupture after the necks propagate through the entire samples. In all cases, the stress–strain curves are highly reproducible prior to rupture. Similar observation is made for five samples cut in the horizontal direction. Apparently, the stress–strain curves of the samples in the two directions differ only by the strain at which the stress rises again after the plateau. Young's modulus is 2.3 ± 0.07 GPa. The strain at which the stress peaks is 0.027 ± 0.03 and the corresponding stress is 56.5 ± 3.8 MPa. The plateau stress is 44.2 ± 1.2 MPa. The strain at which the stress rises again is 2.91 ± 0.05 for the vertical samples, and 3.42 ± 0.02 for the horizontal samples.

Single-edge notched tensile test

We next conduct the single-edge notched tensile (SENT) test (Supplementary Video 2). We record the stress–strain curve, along with snapshots of the sample at several strains (**Figure 4**). At small strains, the stress increases linearly with strain, except for a small deviation in the very beginning, possibly due to some initial misalignment of the sample. At a certain strain, the sample wrinkles and the stress drops somewhat. Shortly after, a white zone emanates from the crack tip. When the stress increases again, the white zone enlarges, but the crack does not advance. As the strain increases further, the crack tip blunts and starts to advance soon after. Then the stress reaches the maximum σ_m. As the crack advances across the sample, the white zone enlarges further and reaches the other side of the sample. Eventually the sample ruptures. We repeat the test using three samples cut in the same orientation,

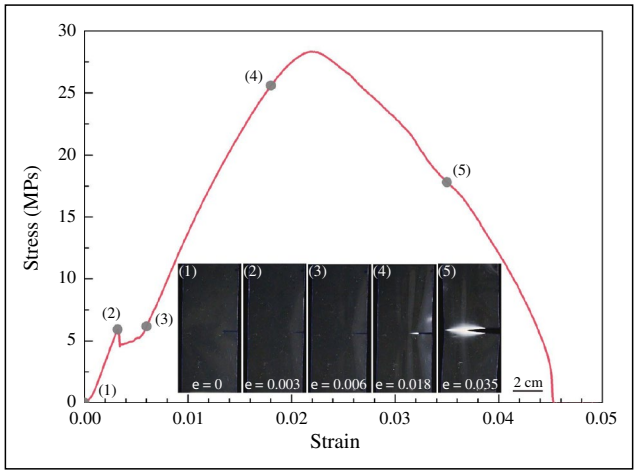

Figure 4. Fracture of a sample containing a precut crack. Stress–strain curve, along with snapshots at several strains. The stress is defined by the applied force divided by the cross-sectional area of the uncut sample. The strain is defined by the displacement of the cross-head divided by the length of the undeformed sample.

and the stress–strain curves of the three samples very nearly coincide.

For the single-edge notch tensile test, the energy release rate is[37]

$$G = \frac{\pi a \sigma^2}{E}\left[1.122 - 0.231\frac{a}{w} + 10.55\left(\frac{a}{w}\right)^2 - 21.71\left(\frac{a}{w}\right)^3 + 30.382\left(\frac{a}{w}\right)^4\right]^2, \quad 3$$

where E is Young's modulus, a is the crack length, and σ is the applied stress (i.e., the applied force divided by the cross-sectional area of the uncut sample). For a crack in a thin sheet, the size of the plastic zone r_p is estimated by[38]

$$r_p = \frac{GE}{2\pi\sigma_Y{}^2}, \quad 4$$

where σ_Y is the yield strength (i.e., the peak stress in Figure 3), which also marks the onset of whitening. Thus, rp is the size of the whitening zone. Equations 3 and 4 are valid when the plastic zone is much smaller than the characteristic length of the sample, such as the crack length. The conditions of small-scale yielding prevail when, say, $r_p < a/25$. Take representative values a = 10 mm, σ_Y = 60 MPa, and E = 2.3 GPa (Figure 3a). The small-scale yielding condition holds when $G < 3900$ J/m^2. As previously noted, the plastic zone for ductile fracture is sometimes comparable to the crack length. Nonetheless, we still use (3) to calculate G. Thus, we should not attach quantitative significance to values of G larger than 3900 J/m^2. Our interest is mostly focused on the brittle fracture caused by hydrolysis, when the plastic zone is small and the energy release rate is low.

The toughness of the PLA film is estimated as follows. We pull a sample with a precut crack in air at a prescribed rate of displacement (Figure 4). The applied stress reaches maximum at $\sigma_m = 28.2 \pm 0.2$ MPa. This maximum stress is used in Figure 4 to estimate the toughness, giving $G_c = 2.45 \pm 0.4 \times 10^4$ J/m^2. As mentioned, this energy release rate violates the small-scale yielding conditions and should therefore not be taken quantitatively.

Hydrolytic crack growth

Hydrolytic crack growth is evaluated by submerging a SENT specimen in an aqueous solution of fixed pH and applying a constant force. (**Figure 5**a). When the crack is short, the energy release rate is low, the crack grows slowly, and the white zone around the crack tip is negligible (Figure 5b). When the crack is long, the energy release rate is high, the crack grows fast, and the white zone is large (Figure 5c). The size of the white zone indicates the extent of plastic deformation. When negligible plastic deformation accompanies the crack growth, the fracture surface is flat, and the thickness of the film near the fracture surface remains nearly unchanged (Figure 5d). When extensive plastic deformation accompanies the crack growth, the fracture surface is porous, and the thickness of the film near the fracture surface reduces substantially (Figure 5e). These general trends are observed for samples subject to various forces and submerged in solutions of various values of pH. Rough and porous fracture surfaces are also observed for a crack growing in air.

The camera records the crack length as a function of time for each sample bearing a constant load in an aqueous solution of a given pH (**Figure 6**). For example, for a sample submerged in a solution of pH 10 and bearing a hanging mass of 500 g, the crack length grows nonlinearly in time (Figure 6b). The crack velocity increases both with crack length and applied load.

When small-scale yielding prevails, the effects of the applied force and the crack length can be combined using a single loading parameter, the energy release rate (3). We plot the velocity of the crack as a function of energy release rate for experiments conducted in solutions of various values of pH and subject to various dead weights (**Figure 7**). Note that small-scale yielding prevails for most data points. For each sample, submerged in a solution of a fixed pH, subject to a dead load, the energy release rate increases as the crack grows. Consequently, the measured crack length as a function of time generates a large number of data points. To display statistical variations, multiple samples are often tested under the same

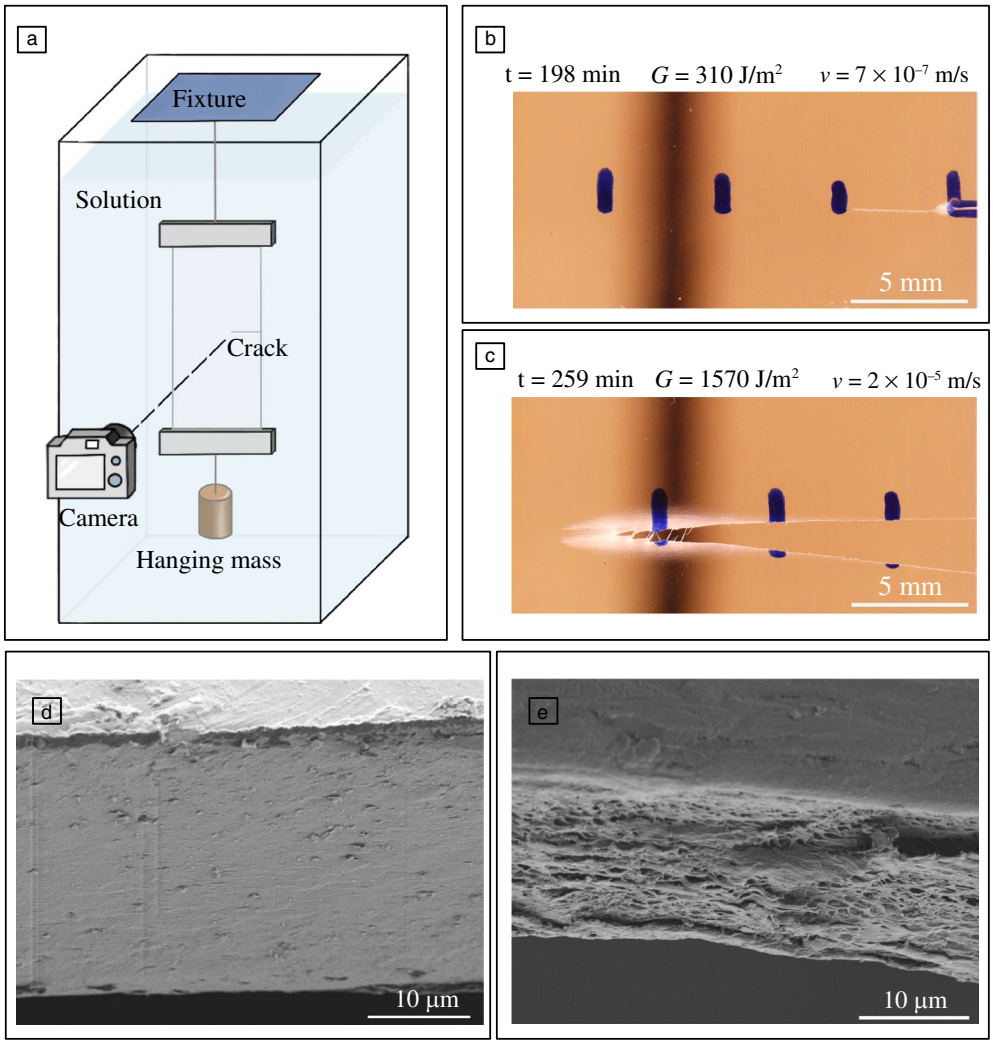

Figure 5. Observation of a crack growing in a sample submerged in a solution of controlled pH. (a) A single-edge notched tensile specimen is submerged in a buffered aqueous solution. A constant force is applied by a hanging mass. The crack growth is monitored using a camera. (b) When a sample is submerged in a buffered aqueous solution of pH 10 and is subject to a hanging mass of 500 g, the crack grows initially with a negligible white zone. (c) As the crack grows longer, the crack grows faster and the white zone becomes larger. (d) Scanning electron microscope (SEM) image of a brittle fracture surface (basic solution, pH 12). (e) SEM image of a ductile fracture surface (deionized water, pH 7).

conditions. We measure crack velocity over about seven orders of magnitude, depending on energy release rate and pH. At a given pH, the crack velocity increases with the energy release rate. For example, at pH 12, we observe that the crack grows under energy release rates ranging from 1.6 to 8000 J/m^2, at velocities ranging from 6×10^{-9} to 6×10^{-4} m/s. For a given pH, when the energy release rate is low, the crack velocity decreases nearly vertically, suggesting that a threshold energy release rate exists, below which the crack does not grow.

Discussion and conclusion

Long polymer chains jam slip

PLA fractures in air by a combination of chain slip and chain scission. When a sample without precrack is stretched, the transparent film turns white, and a neck propagates from one end of the sample to the other end (Figure 3a). The plastic deformation indicates chain slip. After the neck reaches the other end of the sample, the applied force rises again, which indicates that chain slip is jammed.

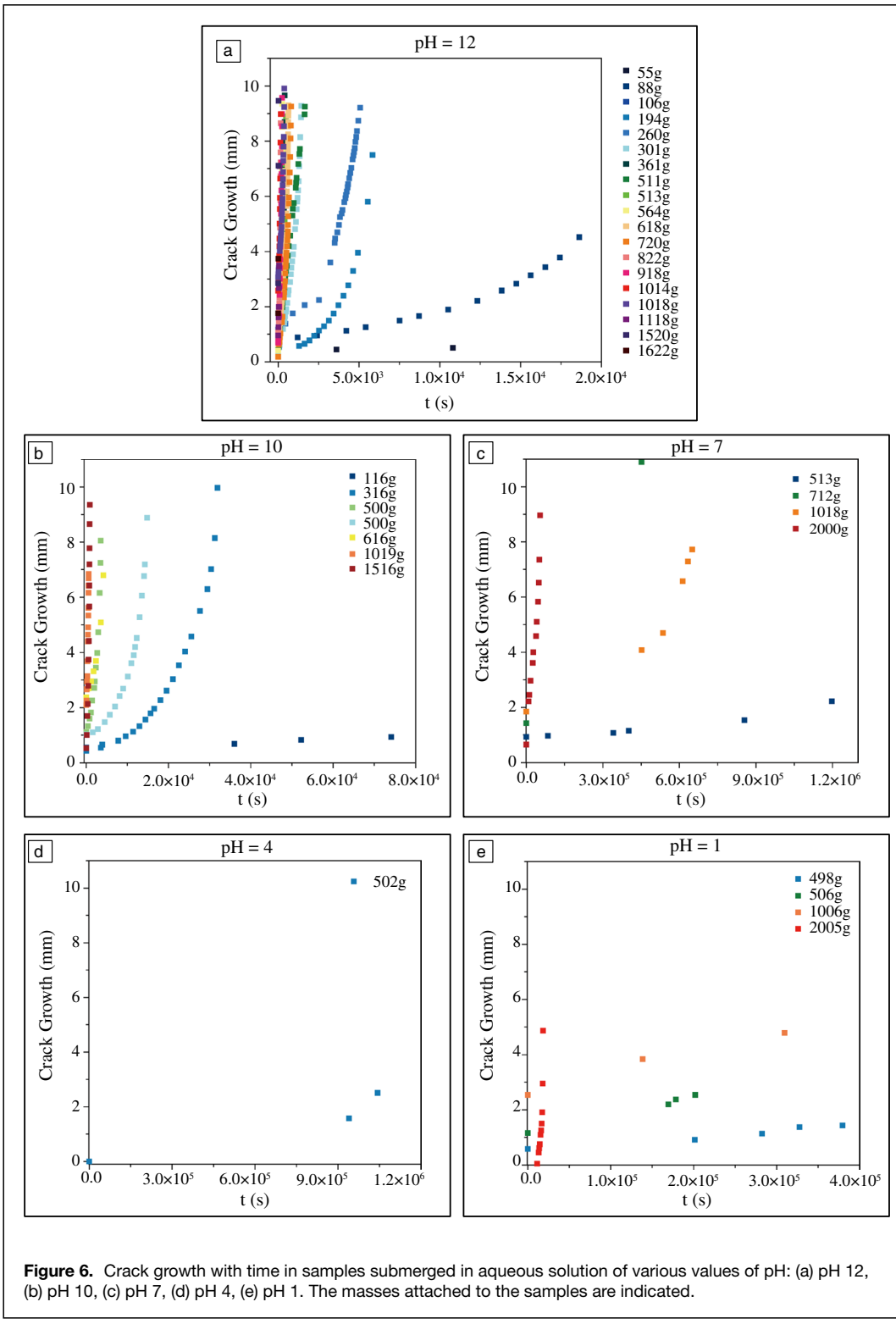

Figure 6. Crack growth with time in samples submerged in aqueous solution of various values of pH: (a) pH 12, (b) pH 10, (c) pH 7, (d) pH 4, (e) pH 1. The masses attached to the samples are indicated.

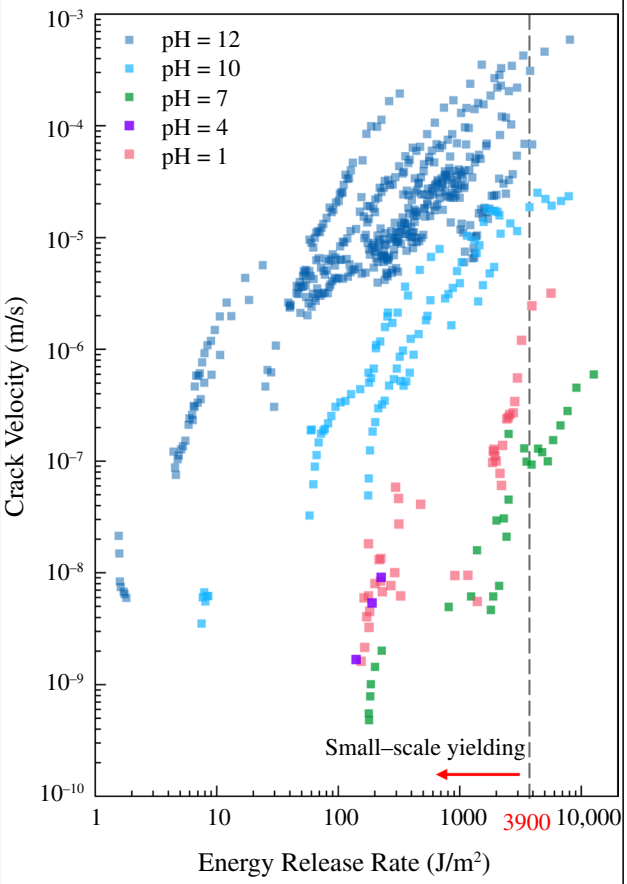

Figure 7. Crack velocity as a function of energy release rate and pH. The dashed line marks the small-scale yielding condition, $G < 3900$ J/m^2.

Whether the sample fractures by chain slip alone or by a combination of chain slip and chain scission can be approximately analyzed by a shear lag model. For simplicity, consider the free-body diagram of a single straight polymer chain, pulled by a stress σ at one end of the chain. As the chain slips relative to other chains, a frictional stress τ acts along the chain, resisting the slip. The balance of forces requires that $\frac{\pi D^2}{4}\sigma = \pi DL\tau$, where D is the diameter and L is the length of the chain, so that $\sigma = 4\tau\frac{L}{D}$. The slip stress τ results from physical interactions between chains. The tensile stress σ is limited by the strength of covalent bonds along the chain. The slip stress is typically orders of magnitude lower than the covalent strength of the chain. The balance of the two forces results from the large ratio L/D. A thermoplastic of a high molecular weight can both undergo substantial chain slip and chain scission.

When the chain is short, the tensile stress in the chain is smaller than the covalent strength, and the sample fractures by chain slip alone (Figure 1b). When the chain is long, the tensile stress can reach the covalent strength, and the sample fractures by a combination of chain slip and chain scission (Figure 1c). We estimate τ by the yield strength, and L/D by the number of repeat units per chain. Taking representative values, $\tau \sim 10^7$ Pa and $L/D \sim 1000$, we estimate that $\sigma \sim 10^{10}$ Pa, which is on the order of the covalent strength. Thus, the chain is long enough to jam slip, building up tension in the chain to break the chain.

Chains slip before scission

In the uniaxial tensile test, a sample undergoes extensive plastic deformation prior to fracture. Similarly, when a sample with a precrack is subject to a tensile force in air, a white zone forms around the crack tip, spreading to the other side of the sample, and then the crack propagates through the sample (Figure 4). The whitening is likely caused by the formation of small voids.[36] SEM imaging shows that the fracture surface is similar to that of a crack growing in a sample submerged in deionized water (Figure 5e), confirming that chains slip extensively before scission.

How can a long polymer chain slip without scission? Depending on how the as-received film is processed, before the film is stretched, each polymer chain is in a more or less relaxed configuration. For simplicity, assume that a polymer chain is initially in a random-walk configuration and carries no tensile stress. When the film is stretched beyond the yield strain, the chain begins to slip relative to other chains, giving rise to plastic deformation. Further assume that the slip stress is constant, specific to the repeat units of the polymer, temperature, and strain rate. For a chain initially in a random-walk configuration, the slip stress along the chain changes direction from one segment of the chain to another. Consequently, the tensile stress in the chain will be small compared to the covalent strength. However, once the chain is jammed, for example by forming a hairpin around another chain, to deform further the two segments of the chain develop slip stress in the same direction along the chain, and the tensile stress in the chain builds up. As more segments of the chain develop slip stress in the same direction along the chain, the tensile stress in the chain builds up further. This process continues until the tensile stress in the chain reaches the covalent bond strength, upon which the chain breaks.

Hydrolysis takes time to break polymer chains

Next consider a sample with a precrack, submerged in an aqueous solution of a given pH, bearing a load. When the crack advances too rapidly for hydrolysis to take place and knock down the covalent strength of polymer chains, chains slip extensively prior to scission, dissipating a substantial amount of energy, leading to a high energy release rate. The SEM image shows a porous fracture surface that is comparable to that formed in deionized water (Figure 5e). When the crack advances slowly enough for hydrolysis to take place and knock down the covalent strength of polymer chains, chains slip negligibly prior to scission, dissipating only a small amount of energy, leading to a low energy release rate. The SEM image shows a smooth fracture surface and negligible thinning of the sample (Figure 5d). Taking these observations

together, we conclude that the PLA film is ductile when the crack advances rapidly, and is brittle when the crack advances slowly. That is, hydrolysis embrittles the PLA. At low crack velocity, hydrolysis causes chain scission by itself, tension in the chains is too small to cause appreciable chain slip, and the energy release rate is low. By contrast, at high crack velocity, hydrolysis cannot cause chain scission by itself, the tension in the chains is high enough to cause appreciable chain slip, and the energy release rate is high. The observed relation between the crack velocity and energy release rate (Figure 7) is commonly interpreted in terms of various mechanisms. For example, the mechanical load opens the crack and allows quick access of water to the crack tip and easy diffusion of debris.[11] Therefore, the energy release rate accelerates the hydrolytic fracture. The stress may also enhance the rate of hydrolysis by reducing the energy barrier, similar to that studied in silica.[20] Another mechanism involves the cooperative effect of stress and ion displacement on the dynamics of cross-link unzipping and rupture of hydrogels.[39] This article reports the hydrolysis-induced embrittlement. Further work is needed to clarify mechanisms.

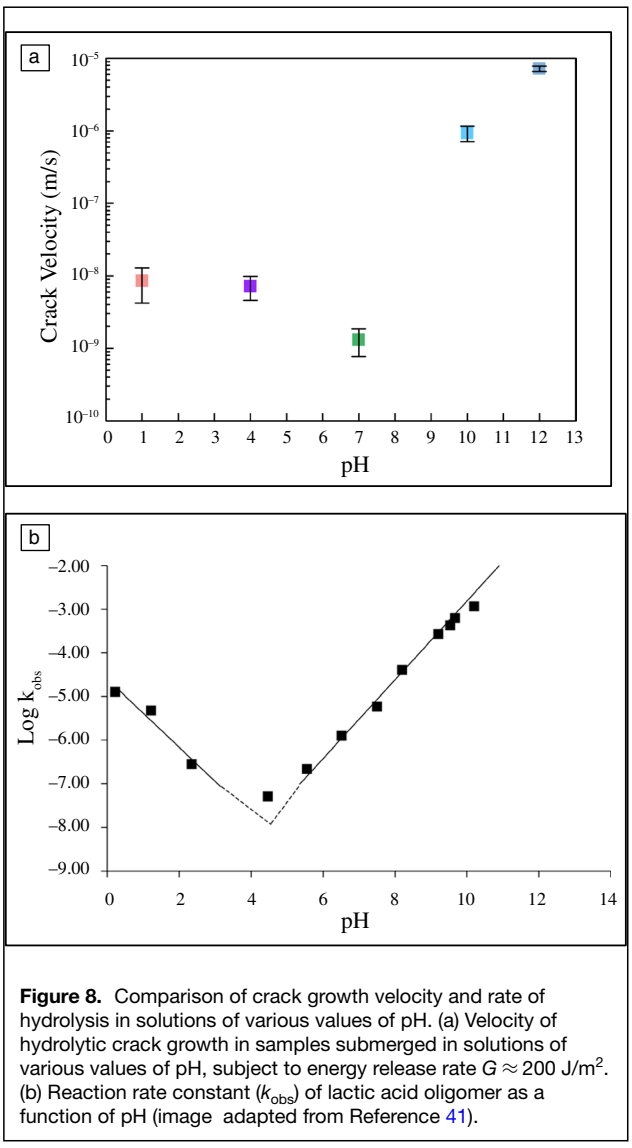

Figure 8. Comparison of crack growth velocity and rate of hydrolysis in solutions of various values of pH. (a) Velocity of hydrolytic crack growth in samples submerged in solutions of various values of pH, subject to energy release rate $G \approx 200$ J/m^2. (b) Reaction rate constant (k_{obs}) of lactic acid oligomer as a function of pH (image adapted from Reference 41).

For environmentally assisted crack growth, crack velocity has been commonly plotted as a function of the energy release rate, or equivalently, the stress intensity factor. The environment can be characterized by, for example, pH, relative humidity, or concentration of ions. For example, Figure 7 for PLA in this article has a similar look to Figure 5 for silica in the classic paper by Wiedenhorn.[40] There are a number of differences. For instance, PLA is ductile compared to silica, which allows us to construct the curve over a significantly large range of energy release rate. We have also observed the transition from ductile to brittle crack growth, which does not occur in silica.

In this article, we characterize the effect of hydrolysis by measuring the crack velocity as a function of energy release rate using samples containing precracks. In design practice, the stress-life curve measured using samples without precracks has also been used. Even a sample without precrack contains small flaws. These small flaws may or may not affect stress-life curves. When hydrolysis prevails, the plastic zone is small, and the small flaws are expected to impact the stress-life curves. When hydrolysis is absent, the plastic zone is large, and the small flaws are not expected to impact the stress-life curves.

Velocity of crack growth in PLA correlates with rate of hydrolysis of lactic acid oligomers

We plot the crack velocity as a function of pH at a low energy release rate, $G \approx 200$ J/m^2 (**Figure 8**a). This function is not monotonic. The crack velocity is high when the solution is either basic or acidic. This observation indicates that H^+ and OH^- both accelerate hydrolytic crack growth. The data show that the basic solution is more effective than the acidic solution. A similar non-monotonic trend is also observed for how pH affects the rate of hydrolysis of lactic acid oligomers[41] (Figure 8b). The crack velocity in samples submerged in the pH 10 solution is ~3 orders higher than in the neutral solution (pH 7). By comparison, the rate of hydrolysis of lactic acid oligomers in the pH 10 solution is ~2.7 orders of magnitude higher than that in the neutral solution. The similarity between the velocity of crack growth and the rate of hydrolysis of oligomers further supports the conclusion that the crack growth at low energy release rate is due to chain scission by hydrolysis. The velocity of a crack and the rate of hydrolysis form a length scale, V/k. A comparison between Figure 8a and b indicates that the length V/k is on the order of millimeters. The significance of this length is not understood at the time of this writing.

PLA is flaw sensitive

Observe that the PLA whitens at a strain about 0.03, when the stress peaks at the upper yield point. At a crack tip, the white region corresponds to the plastic zone, in which chains

slip. The size of this plastic zone, r_p, is estimated by (4). For a sample tested in air, the plastic zone is appreciable compared to the size of the sample.

After yielding, the material starts to form a neck with a small increase in strain (Figure 3a). Note that the strain ~0.03 at which the stress peaks is much smaller than the strain ~3.3 at which the sample fractures. Consequently, at the crack tip, the size of the plastic zone is much larger than the zone in which the neck is well formed. The size of the zone in which the neck is well formed at the crack tip is estimated by

$$r_n = G/W_c, \quad 5$$

where W_c is the work of fracture (i.e., the area under the stress–strain curve up to rupture). This equation should be compared with Equation 4 for the plastic zone size, in which $\sigma_y^2/2E$ is the triangular area under the initial elastic rise of the stress–strain curve. This elastic energy density is about a factor of 100 smaller than W_c, so that $r_p >> r_n$ for a given energy release rate G. When G reaches a value equal to the toughness G_c, the neck breaks at the crack tip and the crack advances. The maximum size of the zone in which the film necks, G_c/W_c, is a material-specific length. Taking representative values for the PLA film used in this work, $W_c = 2.41 \pm 0.29 \times 10^{10}$ J/m^3 and $G_c = 2.45 \pm 0.4 \times 10^4$ J/m^2, we estimate that $G_c/W_c = 10^{-6}$ m. As previously noted, our fracture test violates the small-scale yielding conditions, so that the toughness so determined is inaccurate and we use the value of G_c as an estimate of the order of magnitude.

We observe that the fracture strain measured under uniaxial tension in air varies substantially from sample to sample (Figure 3b). This observation is interpreted as follows. In a tensile test using a sample without precrack, flaws in the sample are inevitable. When a flaw is smaller than the material length G_c/W_c, the fracture strain of the sample is insensitive to the flaw. When a flaw is larger than the material length G_c/W_c, the fracture strain of the sample is reduced by the flaw. As estimated above, the PLA film used in this work has a small material length G_c/W_c, which explains why small flaws can substantially reduce the stretchability of the sample.

In summary, subject to tension in air, a PLA film undergoes large plastic deformation before fracture, indicating extensive slip of polymer chains before scission. We then submerge a PLA film in an aqueous solution of a fixed pH, and observe the growth of a crack in the film under the combined actions of hydrolysis and mechanical load. When the crack grows fast, PLA does not have enough time to hydrolyze. The polymer chains slip extensively before scission by mechanical stress and the energy release rate is high. When the crack grows slowly, PLA has enough time to hydrolyze. The polymer chains slip negligibly before scission by hydrolysis and the energy release rate is low. Under a small energy release rate, how pH affects the velocity of crack in PLA is analogous to how pH affects the rate of hydrolysis of lactic acid oligomers. This observation corroborates that hydrolysis causes the slow crack growth under low mechanical loads. The SEM images show rough and porous fracture surfaces when the crack grows fast, but flat fracture surfaces when the crack grows slowly. This observation further confirms that hydrolysis embrittles PLA. Hydrolytic embrittlement must be taken into account when PLA is used in applications in moist environments. Similar considerations should also apply to all polymers in which the backbones contain bonds susceptible to hydrolysis. These considerations should be taken into account in the development of biodegradable and bioderived polymers.

Acknowledgments

This research was supported by the Harvard University MRSEC, which is funded by the National Science Foundation under Grant DMR-2011754. Part of this work was performed at the Center for Nanoscale Systems (CNS), which is supported by the National Science Foundation under Grant ECS 1541959. M.S. and T.Y. were visiting students at Harvard University supported by the China Scholarship Council. Q.J. acknowledges H. Yang's assistance in sample preparation.

Supplementary Information

The online version contains supplementary material available at https://doi.org/10.1557/s43577-022-00368-5.

References

1. R.E. Drumright, P.R. Gruber, D.E. Henton, Polylactic acid technology. *Adv. Mater.* **12**, 1841 (2000)
2. M.S. Singhvi, S.S. Zinjarde, D.V. Gokhale, Polylactic acid: Synthesis and biomedical applications. *J. Appl. Microbiol.* **127**, 1612 (2019)
3. A. Chamas, H. Moon, J. Zheng, Y. Qiu, T. Tabassum, J.H. Jang, M. Abu-Omar, S.L. Scott, S. Suh, Degradation rates of plastics in the environment. *ACS Sustain. Chem. Eng.* **8**, 3494 (2020)
4. G. Kale, R. Auras, S.P. Singh, Degradation of commercial biodegradable packages under real composting and ambient exposure conditions. *J. Polym. Environ.* **14**, 317 (2006)
5. R. Auras, B. Harte, S. Selke, An overview of polylactides as packaging materials. *Macromol. Biosci.* **4**, 835 (2004)
6. J. Muller, C. González-Martínez, A. Chiralt, Combination of poly(lactic) acid and starch for biodegradable food packaging. *Materials* (Basel) **10**(8), 952 (2017)
7. K. Hamad, M. Kaseem, H.W. Yang, F. Deri, Y.G. Ko, Properties and medical applications of polylactic acid: A review. *Express Polym. Lett.* **9**, 435 (2015)
8. D. da Silva, M. Kaduri, M. Poley, O. Adir, N. Krinsky, J. Shainsky-Roitman, A. Schroeder, Biocompatibility, biodegradation and excretion of polylactic acid (PLA) in medical implants and theranostic systems. *Chem. Eng. J.* **340**, 9 (2018)
9. Y. Song, Y. Li, W. Song, K. Yee, K.-Y. Lee, V.L. Tagarielli, Measurements of the mechanical response of unidirectional 3D-printed PLA. *Mater. Des.* **123**, 154 (2017)
10. T.D. Ngo, A. Kashani, G. Imbalzano, K.T. Nguyen, D. Hui, Additive manufacturing (3D printing): A review of materials, methods, applications and challenges. *Compos. B Eng.* **143**, 172 (2018)
11. X. Yang, J. Steck, J. Yang, Y. Wang, Z. Suo, Degradable plastics are vulnerable to cracks. *Engineering* **7**, 624 (2021)
12. C. Chu, N. Campbell, Scanning electron microscopic study of the hydrolytic degradation of poly (glycolic acid) suture. *J. Biomed. Mater. Res.* **16**, 417 (1982)
13. R. Chandra, R. Rustgi, Biodegradable polymers. *Prog. Polym. Sci.* **23**, 1273 (1998)
14. Z. Wang, M.S. Ganewatta, C. Tang, Sustainable polymers from biomass: Bridging chemistry with materials and processing. *Prog. Polym. Sci.* **101**, 101197 (2020)
15. C. Hepburn, *Polyurethane Elastomers* (Springer, New York, 2012)
16. A. Atrens, N. Winzer, W. Dietzel, Stress corrosion cracking of magnesium alloys. *Adv. Eng. Mater.* **13**, 11(2011). https://doi.org/10.1002/adem.200900287
17. K. Sieradzki, R.C. Newman, Brittle behavior of ductile metals during stress-corrosion cracking. *Philos. Mag. A* **51**, 95 (1985). https://doi.org/10.1080/01418618508245272
18. E. Orowan, The fatigue of glass under stress. *Nature* **154**, 341 (1944). https://doi.org/10.1038/154341a0
19. S.M. Wiederhorn, Moisture assisted crack growth in ceramics. *Int. J. Fract. Mech.* **4**, 171 (1968)

20. M. Ciccotti, Stress-corrosion mechanisms in silicate glasses. *J. Phys. D Appl. Phys.* **42**(21), 214006 (2009). https://doi.org/10.1088/0022-3727/42/21/214006
21. M. Braden, A.N. Gent, The attack of ozone on stretched rubber vulcanizates. I. The rate of cut growth. *J. Appl. Polym. Sci.* **3**, 90 (1960). https://doi.org/10.1002/app.1960.070030713
22. M. Braden, A.N. Gent, The attack of ozone on stretched rubber vulcanizates. II. Conditions for cut growth. *J. Appl. Polym. Sci.* **3**, 100 (1960)
23. M. Shi, J. Steck, X. Yang, G. Zhang, J. Yin, Z. Suo, Cracks outrun erosion in degradable polymers. *Extreme Mech. Lett.* **40**, 100978 (2020). https://doi.org/10.1016/j.eml.2020.100978
24. X. Yang, J. Yang, L. Chen, Z. Suo, Hydrolytic crack in a rubbery network. *Extreme Mech. Lett.* **31**, 100531 (2019). https://doi.org/10.1016/j.eml.2019.100531
25. Q. Jiao, M. Shi, T. Yin, Z. Suo, J.J. Vlassak, Composites retard hydrolytic crack growth. *Extreme Mech. Lett.* **48**, 101433 (2021)
26. T. Baumberger, O. Ronsin, Environmental control of crack propagation in polymer hydrogels. *Mech. Soft Mater.* **2**, 14 (2020). https://doi.org/10.1007/s42558-020-00027-2
27. P. Prentice, The influence of molecular weight on the fracture of thermoplastic glassy polymers. *J. Mater. Sci.* **20**, 1445 (1985)
28. J. Zhao, L. Lu, T. Rabczuk, The tensile and shear failure behavior dependence on chain length and temperature in amorphous polymers. *Comput. Mater. Sci.* **96**, 567 (2015)
29. J. Jancar, E. Fekete, P. Hornsby, J. Jancar, B. Pukánszky, R. Rothon, *Mineral Fillers in Thermoplastics I: Raw Materials and Processing* (Springer, New York, 1999)
30. S.N. Zhurkov, V.E. Korsukov, Atomic mechanism of fracture of solid polymers. *J. Polym. Sci. Polym. Phys. Ed.* **12**, 385 (1974)
31. S.-Q. Wang, S. Cheng, P. Lin, X. Li, A phenomenological molecular model for yielding and brittle-ductile transition of polymer glasses. *J. Chem. Phys.* **141**, 094905 (2014)
32. I. Vroman, L. Tighzert, Biodegradable polymers. *Materials* (Basel) **2**(2), 307 (2009)
33. G.H. Yew, A.M. Yusof, Z.M. Ishak, U.S. Ishiaku, Water absorption and enzymatic degradation of poly (lactic acid)/rice starch composites. *Polym. Degrad. Stab.* **90**, 488 (2005)
34. E.W. Fischer, H.J. Sterzel, G. Wegner, Investigation of the structure of solution grown crystals of lactide copolymers by means of chemical reactions. *Kolloid-Z. Z. Polym.* **251**, 980 (1973)
35. T. Tábi, S. Hajba, J.G. Kovács, Effect of crystalline forms (α′ and α) of poly (lactic acid) on its mechanical, thermo-mechanical, heat deflection temperature and creep properties. *Eur. Polym. J.* **82**, 232 (2016)
36. A. Pawlak, A. Galeski, A. Rozanski, Cavitation during deformation of semicrystalline polymers. *Prog. Polym. Sci.* **39**, 921 (2014)
37. H. Tada, P.C. Paris, G.R. Irwin, *The Stress Analysis of Cracks Handbook* (Del Research Corporation, Hellertown, 1973), p. 53
38. G.R. Irwin, Analysis of stresses and strains near the end of a crack traversing a plate. *J. Appl. Mech.* **24**, 361 (1957)
39. T. Baumberger, O. Ronsin, Cooperative effect of stress and ion displacement on the dynamics of cross-link unzipping and rupture of alginate gels. *Biomacromolecules* **11**, 1571 (2010). https://doi.org/10.1021/bm1002015
40. S.M. Wiederhorn, Influence of water vapor on crack propagation in soda-lime glass. *J. Am. Ceram. Soc.* **50**, 407 (1967). https://doi.org/10.1111/j.1151-2916.1967.tb15145.x
41. S.J. de Jong, E.R. Arias, D.T.S. Rijkers, C.F. van Nostrum, J.J. Kettenes-van den Bosch, W.E. Hennink, New insights into the hydrolytic degradation of poly(lactic acid): Participation of the alcohol terminus. *Polymer* **42**(7), 2795 (2001) □